Miscibility of Isotactic Polypropylene/Ethylene−Propylene Random Copolymer Binary Blends

Motohiro Seki,* Hiroshi Nakano, and Shinichi Yamauchi

Physical and Analytical Science Laboratory 1, Mitsubishi Chemical Corporation, Toho 1, Yokkaichi, Mie, 510-0848 Japan

Jiro Suzuki and Yushu Matsushita

Neutron Scattering Laboratory, Institute for Solid State Physics, The University of Tokyo, Shirakata 106-1, Tokai, Naka, Ibaraki, 319-1106 Japan

Received August 7, 1998; Revised Manuscript Received January 6, 1999

ABSTRACT: Miscibility for blends of isotactic polypropylene (PP) and ethylene-d_4−propylene random copolymer (EPR)s prepared by copolymerization of propylene and perdeuterated ethylene with metallocene catalyst has been investigated by small-angle neutron scattering (SANS). SANS experiments were conducted for the blends of PP with EPRs containing 19 mol % (D-EPR19) and 47 mol % (D-EPR47) of deuterated ethylene unit at various temperatures. SANS results indicated that most of the blends are in the homogeneous one-phase mixture, and the Flory−Huggins interaction parameter χ analyzed by the random phase approximation is approximately 5.0×10^{-3} for the PP/D-EPR47 blend while it is very small and within the range $-1.0 \times 10^{-3} \leq \chi \leq 1.0 \times 10^{-3}$ for the PP/D-EPR19 blend. It was also revealed that χ does not change with temperature meaningfully within the temperature range $440 \leq T \leq 482$ K, while phase separation due to crystallization of PP was observed at 373 K. No domain structure of EPR whose size is in the range of an optical microscope was observed by TEM for the blends quenched from the melt.

I. Introduction

Miscibility between olefinic copolymers has been studied by many researchers experimentally and theoretically.[1−15] The origin of miscibility between different polyolefins has been explained by both enthalpic[3−7,12] and entropic[9,10] interactions.

Krishnamoorti et al.[3] have found that the difference in the solubility parameter between two random copolymers, which have been provided by hydrogenation of polybutadiene, evaluated by thermal expansion coefficient and isothermal compressibility correlates fairly well with that from the interaction parameter χ measured by SANS. It suggests that interactions between polyolefins are largely enthalpic in nature. On the other hand, Bates et al.[9,10] showed that the changes in nonlocal packing that are accompanied by the mixing of chains with distinct Gaussian conformation are the origin of interaction, since the enthalpic interaction between the saturated hydrocarbons is so small that it may be ignored.

Because of the importance in industrial aspects and scientific interests, miscibility for the blends of isotactic polypropylene (PP) with other olefinic copolymers has been studied intensively with various techniques such as SANS,[8,13] SALS,[14,15] NMR,[16] micrography,[17−20] and dynamic mechanical analysis.[20] Weimann and co-workers[8] revealed that atactic poly(ethylene−ethylethylene) random copolymers containing 73−90 wt % 1-butene should be miscible with PP in the melt, and compatibility studies by Yamaguchi et al.[20] suggested that the poly(ethylene−butene)s with 56 and 62 mol % 1-butene content, which were obtained with metallocene catalyst, showed a better compatibility with PP in mechanically mixed melt blends than poly(ethylene−butene) with a smaller 1-butene content based on the results of the dynamic mechanical analysis and TEM observations. It was also revealed that the blends of PP and ethylene−propylene−diene terpolymer, which contained 70 wt % of ethylene and 5 wt % of ethylenenorbornene, have a lower critical solution temperature and are miscible in a limited temperature gap by means of SALS.[15] Furthermore, miscibility between i-PP and other stereoisomers has been studied.[13,21] A blend of PP with atactic PP is miscible in the melt,[13] and phase separation occurs on crystallization of PP because of the lack of crystallizability of atactic PP, while it was concluded that miscibility between isotactic and syndiotactic PP was very low from the results of the crystallization kinetics.[21]

Miscibility of isotactic PP and ethylene−propylene random copolymer (EPR), whose chemical sequence is below, has also been studied, and it was concluded that these are immiscible in the melt.[13,14,16,17] Previous SANS experiments[13] for the blends of PP and EPRs were immiscible in the melt (200 °C), even the case where EPR contained only 8% of ethylene.

PP: $-(CH_2-CHCH_3)_x-$

EPR: $-(CH_2-CH_2)_y- -(CH_2-CHCH_3)_{(1-y)}-$

In the past decade, remarkable developments on metallocene catalyst have enabled us to obtain fairly homogeneous and statistically random copolymers. EPRs polymerized with metallocene catalyst are rather homogeneous in terms of ethylene content, and so ethylene units are distributed more randomly in a chain than those prepared with the Ziegler−Natta[22] catalyst. Further EPRs prepared from metallocene catalyst have more configurational regularity for the sequential methyl group than those polymerized by a vanadium-based catalyst[22,23] because of the steric restriction on polymerization at the metal center. In the present study, miscibility of PP and deuterated EPRs with two differ-

10.1021/ma981254w CCC: $18.00
Published on Web 04/28/1999

Table 1. Molecular Characteristics of Polypropylenes

sample	M_w[a] (g/mol)	N_w	M_w/M_n[a]	density[b] (g/cm^3)	[mmmm][c] (mol %)	R_g[d] (nm)	$R_g/M_w^{1/2}$ (nm mol$^{1/2}$ g$^{-1/2}$)
PP-1	6200	148	1.80	0.908_7	98.0	2.5_0	0.032
PP-2	9100	217	1.90	0.908_6	98.0	2.9_5	0.031

[a] Determined by GPC-MALLS. [b] By density gradient column at 25 °C. [c] Isotactic pentad fraction determined by ^{13}C NMR. [d] *z*-averaged radius of gyration evaluated by SANS.

ent ethylene contents (19 and 47 mol %), polymerized by metallocene catalyst, were investigated at various temperatures in the melt and below the melting temperature of PP by SANS. Morphologies of the blends in the solid were also studied by small-angle X-ray scattering (SAXS), differential scanning calorimetry (DSC), and transmission electron microscopy (TEM).

II. Experimental Section

Preparation of Polymers. Isotactic polypropylene (PP) samples were prepared with the Ziegler−Natta catalyst. Low molecular weight fractions were extracted from as-polymerized products with boiling *n*-hexane for 3 h. The two extracted fractions were precipitated into methanol followed by drying under vacuum; they were named PP-1 and PP-2, respectively. Their isotacticities were measured with a JEOL NMR model JNM-GSX270 and are listed in Table 1.

The polymerization of EPR containing 47 mol % of ethylene (H-EPR47) was performed as follows: A 1 L stainless steel vessel was evacuated and purged several times with monomer−gas mixture (ethylene:propylene:hydrogen = 49.6:49.6:0.8 (mol)) by pressurizing and venting. After 500 mL of *n*-heptane was added at 338 K, the pressure was adjusted at 1.0 kg/cm^2 by adding the monomer−gas mixture. The solution of methylisobutylalmoxane (Al/Zr = 1000 (mol/mol)) and a toluene solution of dimethylsilylenebis(2-methyl-4,5-benzoindenyl)-zirconium dichloride (5.0×10^{-6} mol) were injected to this reactor. Then the pressure was elevated to 1.2 kg/cm^2 and held constant by further additions of monomer−gas mixture. After the polymerization performed for 83 min at 338 K, the reactor was opened in the atmosphere. The solvent was removed by evaporation at 348 K in N_2 atmosphere. A similar procedure was applied for other polymerization in order to obtain EPR containing 18 mol % of ethylene (H-EPR18) and also to obtain labeled EPRs with 19 mol % (D-EPR19) and 47 mol % (D-EPR47) of ethylene-d_4. Those were prepared by using perdeuterated ethylene (C_2D_4) instead of regular ethylene (C_2H_4). As-polymerized EPRs were dissolved in chloroform, and then the solutions were filtered with a membrane three times to remove the rest of catalyst and then placed under vacuum to remove the solvent and voids.

Determination of Ethylene Content and Microstructure of EPR. ^{13}C NMR spectra for parent EPRs were obtained to determine ethylene content and microstructure[23] with a JEOL GSX-270 spectrometer. The samples were run at 403 K as 40% (vol/vol) solutions in *o*-dichlorobenzene with benzene-d_6 as the lock material. Experiments were performed using a pulse sequence of the inverse gated decoupling method.[24] Molecular weight dependence of ethylene content was also checked by GPC connected with on-line FTIR by measuring the intensities of IR absorption peaks at 2955, 2927, and 2180 cm^{-1}, which are ascribed to $-CH_3$, $\rangle CH_2$, and $\rangle CD_2$, respectively.[25] These peak intensity ratios at different elusion time should indicate the variation of ethylene content with different molecular weight. The variation was determined to be quite small and can be estimated less than ±1.5 mol %.

All of these parent EPRs were fractionated with a preparative GPC (Japan Analytical Industry Co., Ltd. model LC-908 with a column of JAIGEL-3H-A) from chloroform solution. Fractionated samples were coded H-EPR47a-c, D-EPR47a-c, H-EPR18a-b, and D-EPR19a-b, where H and D indicate unlabeled and labeled EPR, respectively. The numbers in the sample codes denote the ethylene content expressed in mole percent and added letters a, b, and c mean fractions.

Table 2. Characterization Data of Parent EPRs

sample	M_w/M_n[a]	ethylene content (*y*)[b]	[PPP][c] (mol %)	[mm][d] (mol %)	ΔC_2[e] (mol %)	density[f] (g/cm^3)
H-EPR47	2.20	47	20	57	+1.5	0.855_0
D-EPR47	2.10	47			<±0.5	0.899_6
H-EPR18	2.10	18	63	82	+0.5	0.876_8
D-EPR19	2.10	19			+0.5	0.881_9

[a] By GPC. [b] By ^{13}C NMR. [c] The fraction of the propylene triad by ^{13}C NMR. [d] The fraction of meso triad for propylene triad by ^{13}C NMR. [e] The variation of ethylene content determined by GPC/FTIR. [f] By density gradient column.

Measurement of Molecular Weight. Weight-averaged molecular weight (M_w) and polydispersity of molar mass for PPs and fractionated EPRs were measured by a GPC with on-line multiangle laser light scattering photometer (GPC-MALLS) at 413.2 K. The GPC system is a Waters model 150C with three polystyrene columns (SHODEX KF-806M from Showa Denko Co. Ltd.,). A 0.3 mL aliquot of 1,2,4-trichlorobenzene solution of the sample with concentration of 2 mg/mL was injected at flow rate of 1.0 mL/min. The differential refractometer was used to detect solute concentrations and specific refractive index increments. The MALLS model DAWN DSP from Wyatt Technology Corp., equipped with a He−Ne laser ($\lambda_0 = 632.8$ nm), was connected with the GPC instrument. ASTRA software package from Wyatt Technology Corp. was used for analyzing GPC data and scattering data, which were collected simultaneously at 17 scattering angles ranging from 18° to 155°. M_w's were evaluated by the method of Zimm, and weight-averaged degree of polymerizations (N_w) of samples were defined by dividing M_w by molar mass of repeat unit, i.e., $M_w/42$, $M_w/(28y + 42(1 - y))$ and $M_w/(32y + 42(1 - y))$, for PPs, H-EPR, and D-EPR, respectively, *y* being ethylene mole fraction.

Density Measurements. Densities of PPs and parent H- and D-EPRs at room temperature were measured by a density gradient column. To evaluate the temperature dependence of density of these samples, dilatometry were performed at temperatures ranging from 313 to 503 K. Specific volume was recorded at the temperature interval of ca. 10 K. We assumed that fractionated EPRs have the same specific volume of parent EPR in the melt because the differences in ethylene content for each fraction were small. The specific volumes of polymers at certain temperature were estimated from the linear interpolation of two neighboring measured values.

Small-Angle Neutron Scattering. PP-1 and PP-2 were dissolved in mixed solvent of decahydronaphthalene (DHNA) and deuterated *p*-xylene (C_8D_{10}) (*p*-xylene:DHNA = 3:2 vol) at different concentrations at 402 K in order to measure the *z*-averaged radius of gyration $R_{g\langle z\rangle}$. To prevent the degradation of polymers, 0.1 wt % of commercially antioxidant (IRGANOX1010 from Cyba) was added to all samples used in this study.

Fractionated H- and D-EPR with almost the same degree of polymerization and ethylene content were weighted and then dissolved in chloroform to prepare a homogeneous equal volume mixture, followed by placing under vacuum at room temperature. Blends of labeled and unlabeled EPRs were named with ethylene content of D-EPR and fraction code, that is 47a-c and 19a-b, and they are listed in Table 3. PP/D-EPR blend samples were prepared by dissolving polymers in toluene at 393 K, followed by precipitation in cold methanol. The precipitates were filtered out and then dried under vacuum for 2 days at room temperature. All blends were press molded at room temperature and were sandwiched between a quartz and an aluminum disk for SANS experiments. PP/D-EPR blends are summarized in Table 4.

SANS experiments were carried out on the SANS-U spectrometer of the Institute for Solid State Physics, University of Tokyo, in JRR-3M at Tokai. The experiments were con-

Table 3. Molecular Characterization of Fractionated EPRs

H/D blend	fractionated H-EPR			fractionated D-EPR			R_g[c] (nm)	$R_g/\langle M_w\rangle^{1/2}$ [d] (nm mol$^{1/2}$ g$^{-1/2}$)
	sample	$N_{w,H}$[a]	M_w/M_n[b]	sample	$N_{w,D}$[a]	M_w/M_n[b]		
47a	H-EPR47a	105	1.16	D-EPR47a	119	1.10	2.3_7	0.038
47b	H-EPR47b	265	1.07	D-EPR47b	261	1.13	3.8_4	0.040
47c	H-EPR47c	1201	1.23	D-EPR47c	1360	1.24	8.4_1	0.040
19a	H-EPR18a	258	1.18	D-EPR19a	266	1.21	3.6_2	0.036
19b	H-EPR18b	458	1.18	D-EPR19b	415	1.13	4.8_1	0.037

[a] Weight-averaged degree of polymerization evaluated by M_w and molar mass of repeat unit. [b] By GPC-MALLS. [c] z-averaged radius of gyration evaluated by SANS data based on eq 8. [d] $\langle M_w\rangle$ is a geometric mean of $M_{w,H}$ and $M_{w,D}$.

Table 4. Blend Samples and SANS Results

blend	PP		fractionated D-EPR				
	sample	ϕ_{PP}[a]	sample	ϕ_{D-EPR}[b]	$\chi_{PR} \times 10^3$ [c]	$\chi_s \times 10^3$ [d]	temp (K)
PP-1/D-EPR47b(80:20)	PP-1	0.825	D-EPR47b	0.175	5.5 ± 0.5	15.6	487
PP-1/D-EPR47b(60:40)	PP-1	0.615	D-EPR47b	0.385	3.8 ± 0.5	10.5	479
PP-2/D-EPR47a(90:10)	PP-2	0.900	D-EPR47a	0.100	5.0 ± 1.0	47.9	478
PP-2/D-EPR47c(80:20)	PP-2	0.810	D-EPR47c	0.190	*e*	4.7	478
PP-1/D-EPR19a(80:20)	PP-1	0.820	D-EPR19a	0.180	$<\|1.0\|$	14.7	478
PP-1/D-EPR19b(80:20)	PP-1	0.815	D-EPR19b	0.185	-1.0 ± 0.5	10.7	463
PP-1/D-EPR19b(60:40)	PP-1	0.610	D-EPR19b	0.390	$<\|1.0\|$	8.5	467

[a] Volume fraction of PP. [b] Volume fraction of D-EPR. [c] Interaction parameter between PP and D-EPR by SANS. [d] Thermodynamical stability limit (χ_s), which is given by eq 9. [e] Equation 7 does not hold.

ducted with cold neutrons whose wavelength λ was 0.7 nm with its distribution $\Delta\lambda/\lambda$ of 0.1 and a sample-to-detector distance of 2 or 4 m. Absolute intensity calibration was accomplished with a Lupolene standard which has been already calibrated.[26] All scattering patterns were azimuthally averaged due to the isotropy so as to produce one-dimensional plots of absolute intensity versus the magnitude of the scattering wave vector $|\mathbf{q}| = 4\pi \sin(\theta)/\lambda$, where 2θ is the scattering angle. Further details for calibration and data reduction methods have been given elsewhere.[26]

All samples except PP solutions were placed under vacuum to avoid the degradation. Experiments were made thermally equilibrated prior to acquisition of SANS data, by holding for 0.5 h at each experimental temperature which was controlled with a computer within accuracy of ±0.01 K.[26] Data of PP solutions were collected at 402 K to avoid the vaporization of the solvent, while the mixtures of labeled and unlabeled EPRs were examined at 433 K. Measurements on blends of PP and D-EPR in the melt were performed at different temperatures ranging from 440 to 482 K; the temperature range was restricted by the melting point of PP and the upper limit of sample holder equipment. SANS experiments were also performed at 373 K; PP crystallizes under this temperature.

TEM Observation. The blends of PP and D-EPR which were prepared as for SANS experiments were placed between the thin glass plates for 10 min at 483 K and then put into the dry ice−ethanol immediately. Thin films were about 10−25 μm in thickness. Only for PP-1/D-EPR19b(60:40) was the blend isothermally crystallized for 1 h at 373.4 K after holding for 10 min at 493 K. These samples were sectioned into slices with thickness of about 80 nm after staining with ruthenium tetroxide for 3 h at room temperature. TEM observation was carried out using a JEOL TEM model JEM 100CX.

Small-Angle X-ray Scattering (SAXS). To investigate the solid-state morphology, PP-1, PP-1/D-EPR47b(80:20), and PP-1/D-EPR19b(80:20) were isothermally crystallized at 373 K for 2 h from the melt (483 K). SAXS from the sample was measured with a rotating-anode X-ray generator from Rigaku ULTRAX-18 operated at 45 kV and 275 mA. Monochromated Cu Kα ($\lambda = 0.154$ nm) was point-collimated by three pinhole slits. The intensity of scattered X-rays by the samples was recorded with a position-sensitive linear detector. The sample-to-detector distance was 1.40 m.

DSC Measurements. In a differential scanning calorimeter (Perkin-Elmer calorimeter DSC-7) the PP and the blends used for SAXS measurement were heated from 293 to 493 K at a scanning rate of 20 K/min in N_2 atmosphere. Crystallinity (X_c) of PP in the blend samples was determined from the division of the heat of fusion per gram of PP by that of a perfect crystalline PP (209 J/g).[27]

III. Analysis of SANS Data

The coherent cross section ($d\Sigma/d\Omega$) from PP solution in a deuterated solvent is given by[28−30]

$$\frac{d\Sigma}{d\Omega} = (a_P - a_S v_P/v_S)^2 S(q) \tag{1}$$

where a_P and a_S[31] are coherent scattering lengths of monomer of PP and of the deuterated solvent molecule, while v_P and v_S are specific molar volume of PP and molar volume of the solvent, respectively. In eq 1, $S(q)$ denotes the pair correlation function including structure factor of PP molecule. $S(q)$ of a polymer particle in a dilute solution at small q region can be given by eq 2,[34]

$$S(q) \propto \exp(-q^2 R_{g\langle z\rangle}^2/3) \quad \text{for } qR_{g\langle z\rangle} < 1 \tag{2}$$

where $R_{g\langle z\rangle}$ is the z-averaged radius of gyration. Subscript $\langle z\rangle$ of the radius of gyration of a solute, PP molecule in this case, will be omitted to simplify the notation and $R_{g\langle z\rangle}$ will be simply written R_g hereafter in this paper. R_g of PP can be evaluated from eqs 1 and 2.

For a homogeneous mixture of labeled and unlabeled EPR, the coherent cross section is given by eq 3,

$$\frac{d\Sigma}{d\Omega} = (a_H/v_H - a_D/v_D)^2 S(q) \tag{3}$$

where a_D and a_H are the scattering lengths of monomers of the labeled and unlabeled EPR, which have the specific molar volumes v_D and v_H, respectively. The structure factor $S(q)$, based on the random phase approximation (RPA), is given by eq 4,[32]

$$\frac{1}{S(q)} = \frac{1}{v_H N w_H \phi_H P_H(q^2 R_{g,H}^2)} + \frac{1}{v_D N w_D (1-\phi_H) P_D(q^2 R_{g,D}^2)} - \frac{2\chi_{HD}}{v_0} \tag{4}$$

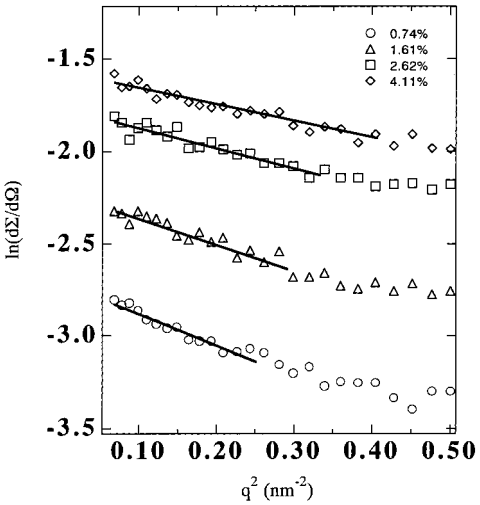

Figure 1. Guinier plots for the solutions of PP-1 with different concentrations at 402 K. Concentrations of the solutions are 0.74% (circles), 1.61% (triangles), 2.62% (squares), and 4.11% (diamonds).

where ϕ_H is the volume fraction of the unlabeled EPR and $N_{w,H}$, $N_{w,D}$, $R_{g,H}$, and $R_{g,D}$ are the weight-averaged degree of polymerization and radii of gyration of the unlabeled and labeled EPR. The reference volume v_0 is defined as $v_0 = (v_H v_D)^{1/2}$ and χ_{HD} denotes the Flory–Huggins interaction parameter between segments of two species. In eq 4 the particle scattering factors, $P_D(q^2R_{g,D}^2)$ and $P_H(q^2R_{g,H}^2)$ were assumed to be represented by the Debye function,[33]

$$P_i(X_i) = \frac{2}{X_i^2}[\exp(-X_i) - 1 + X_i] \tag{5}$$

where X_i denotes $q^2R_{g,i}^2$ and subscript i is H or D.

If we assume unlabeled and labeled EPR are identical except labeling, we can set $v_H = v_D = v$ and $N_{w,H} = N_{w,D} = N_w$, accordingly $R_{g,H} \equiv R_{g,D} \equiv R_g$, and hence $P_H(X_H) \equiv P_D(X_D) \equiv P(X)$. These simplify eq 4 considerably to eq 6.

$$\frac{1}{S(q)} = \frac{1}{v\phi_H(1-\phi_H)N_wP(X)} - \frac{2\chi_{HD}}{v} \tag{6}$$

R_g of EPR can be evaluated precisely from eq 3, 0.5 and 6, since the second term on the right-hand side in eq 6 is negligible because χ_{HD} should be expected to be small for the present H-EPR/D-EPR blends.

Expanding the idea of RPA to the miscible blend of PP and D-EPR, eq 4 can be rewritten as eq 7 using eq 5,

$$\frac{1}{S(q)} = \frac{1}{v_P N_{w,P}\phi_P(q^2R_{g,P}^2)} + \frac{1}{v_R N_{w,R}(1-\phi_P)P_R(q^2R_{g,R}^2)} - \frac{2\chi_{PR}}{v_0} \tag{7}$$

where subscripts P and R denote PP and D-EPR.

IV. Results and Discussion

M_w, polydispersity, and isotacticiy of PPs are listed in Table 1. In Figure 1 natural logarithms of background corrected coherent cross sections for PP-1 solutions with different concentration are plotted against q^2. By extrapolation of R_g value estimated from the initial slopes at low q range ($qR_g < 1$) in Figure 1 to zero concentration, R_g's for PPs were determined as shown in Figure 2 and are listed in Table 1.

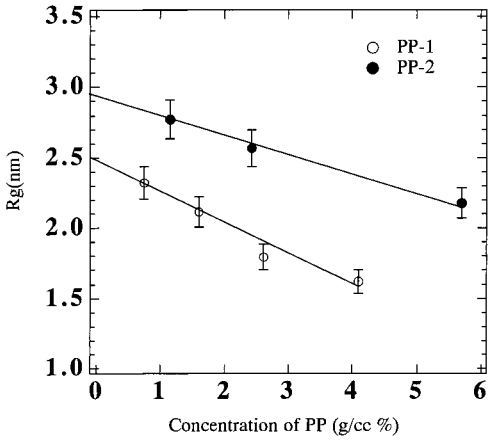

Figure 2. Concentration dependence of z-averaged radius of gyration for PP-1 (open circles) and PP-2 (closed circles).

Molecular characteristics of labeled and unlabeled parent EPRs are listed in Table 2. H-EPR18 containing 18 mol % of ethylene has as much as 82% of meso triad [mm] for propylene triad [PPP]. Propylene units in EPR molecules have an isotactic sequence because the metallocene catalyst restricts the orientation of the methyl group during the polymerization reaction,[22,38,39] but microstructures for D-EPRs were not able to be evaluated due to coupling of NMR signal from D and ^{13}C. D-EPR19 is slightly denser than H-EPR18 as H-EPR18 has a higher crystallinity than D-EPR19; this compensates for the effect of deuteration.

In Table 3 characterization data for the fractionated EPRs and equal volume blends of labeled and unlabeled EPR are summarized. Since N_w's of fractionated H- and D-EPR for each pair are almost the same, the difference being within 13%, and v_H are identical with v_D within the experimental errors even for the blends of H-EPR18 and D-EPR19, it is reasonable to assume that the H-EPR and D-EPR used for the blends have the same R_g ($R_{g,H} \equiv R_{g,D}$), resulting in $P_H(X_H) \equiv P_D(X_D) \equiv P(X)$. Equation 6 can be rewritten as eq 8,

$$\frac{1}{S(q)} = \frac{1}{v\phi_H(1-\phi_H)\langle N_w\rangle P(X)} - \frac{2\chi_{HD}}{v} \tag{8}$$

where $\langle N_w\rangle$ is a geometric mean of $N_{w,H}$ and $N_{w,D}$.

Figure 3 shows background corrected SANS data for the blends of labeled and unlabeled copolymer containing 47 mol % of ethylene unit. All of the coherent cross sections are well fitted to RPA formalism (eq 8) using fitting parameters, i.e., R_g and χ_{HD}. The interaction parameter χ_{HD}, obtained from the best fit to eq 8, was very small as expected and being for all blends. Consequently, χ_{HD} was neglected on evaluating R_g and then are listed in Table 3. $R_g/\langle M_w\rangle^{1/2}$ values are around 0.040 and 0.037 nm mol$^{1/2}$ g$^{-1/2}$ for blends of H-EPR47/D-EPR47 and H-EPR18/D-EPR19, respectively. These values are between those for polyethylene (0.048) and isotactic PP (0.034).[35]

Characteristics of PP/D-EPR blends are listed in Table 4. In Figure 4 background corrected SANS data for PP-1/D-EPR47b (80:20) are plotted as a function of q. As the temperature dependence of radius of gyration $|\partial \ln \langle R_g^2\rangle/\partial T|$ is in generally known to be small and is

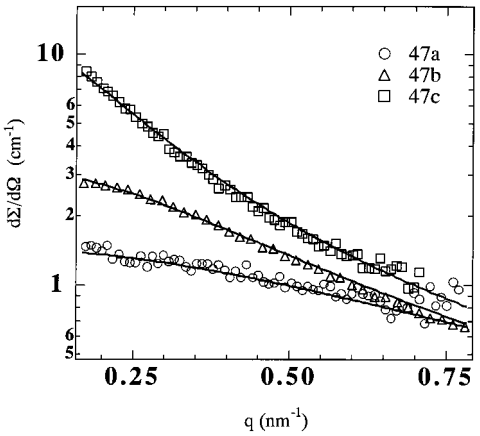

Figure 3. Background-corrected SANS results for equal volume blends of fractionated H and D-EPRs at 433 K: 47a (circles), 47b (triangles), and 47c (squares). Solid curves represent best fit of data sets using eq 8, with an adjustable parameter R_g neglecting the χ_{HD}.

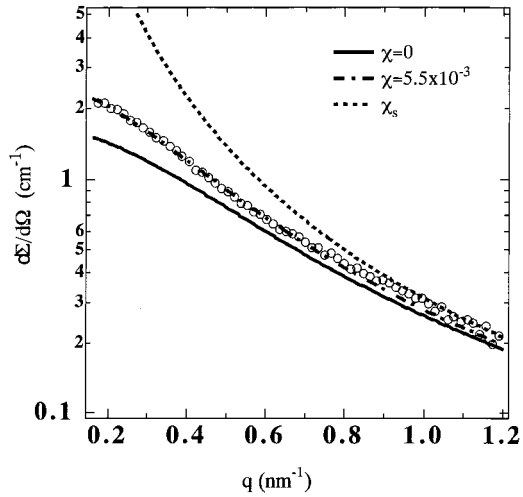

Figure 4. Background-corrected SANS intensities for PP-1/D-EPR47b (80:20) at 487 K. Solid line and dotted line have been calculated for the limits of ideal mixing ($\chi = 0$) and stability limit ($\chi = \chi_s$) based on eq 7, respectively. Dashed−dotted line corresponds to the best fit ($\chi = 5.5 \times 10^{-3}$).

on the order of 1.0×10^{-3} K^{-1},[35,36] R_g's of EPRs at 433 K and of PPs at 402 K were used on analyzing the SANS results for blends of PP and D-EPR. χ for *regular* homogeneous olefin polymer blends is normally expected to be between the athermal limit and stability limit; that is, within the range $0 \le \chi \le \chi_s$. χ_s is given by[32] eq 9.

$$\chi_s = \frac{v_0}{2}\left(\frac{1}{v_P N_{w,P} \phi_P} + \frac{1}{v_R N_{w,R}(1-\phi_P)}\right) \qquad (9)$$

χ_s for PP-1/D-EPR47b (80:20) was estimated to be 15.6 $\times 10^{-3}$ by using 8.023×10^{-23} cm^3, 9.431×10^{-23} cm^3, 8.699×10^{-23} cm^3, 148, 261, and 0.825 for v_R, v_P, v_0, $N_{w,P}$, $N_{w,R}$, and ϕ_P, respectively. By introducing $N_{w,P}$ and $R_{g,P}$ in Table 1 and $N_{w,R}$ and $R_{g,R}$ in Table 3 to eq 7, the interaction parameter between PP and D-EPR, χ_{PR}, can be evaluated by curve fitting. χ_{PR} for all blends are summarized in Table 4. In Figure 4 experimental SANS data for PP-1/D-EPR47b (80:20) is apparently between the line for $\chi = 0$ (solid line) and that for $\chi_s = 15.6 \times 10^3$ (dotted line), and the best fit to eq 7 results in $\chi_{PR} = (5.5 \pm 0.5) \times 10^{-3}$. Similar χ_{PR} values are obtained for PP-1/D-EPR47b (60:40) as shown in Figure 5 and

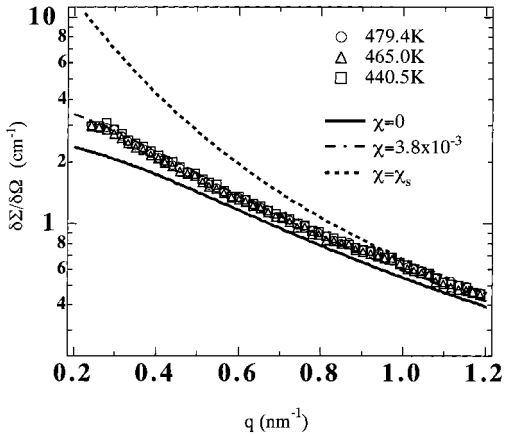

Figure 5. Background-corrected SANS intensities for PP-1/D-EPR47b (60:40) at different temperatures: 440.5 K (squares), 465.0 K (triangles), and 479.4 K (circles). Solid line and dotted line have been calculated for $\chi = 0$ and for $\chi = \chi_s$. Dashed−dotted line corresponds to the best fit ($\chi = 3.8 \times 10^{-3}$).

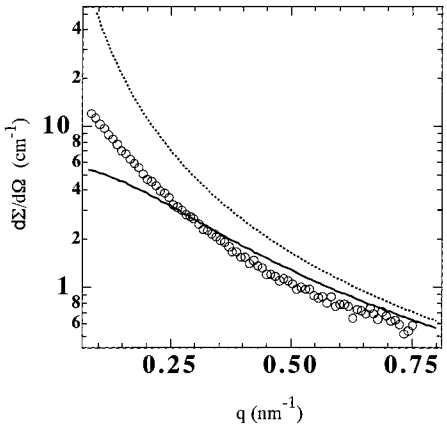

Figure 6. Background-corrected SANS intensities for PP-2/D-EPR47c (80:20) at 478 K. Solid line and dotted line have been calculated for $\chi = 0$ and for $\chi = \chi_s$, respectively.

also for PP-2/D-EPR47a (90:10).

On the other hand, χ_s for PP-2/D-EPR47c (80:20) is 4.7×10^{-3}, which is comparable to χ_{PR} for three blends from the top in Table 4. Accordingly, the coherent cross section for PP-2/D-EPR47c (80:20) at 478 K shown in Figure 6 cannot be expressed by eq 7 for large q ($q \ge 0.3$ nm^{-1}), being lower than predicted. This fact suggests that phase separation occurs in this system. Allamo et al.[37] calculated that the scattering intensity from a two-phase polymer melt at high q should always be lower than that of a homogeneous one-phase mixture with the same composition.

In Figure 7 SANS data for PP-1/D-EPR19b (80:20) at 463 K are plotted against the scattering vector. As is clearly shown in the figure, the interaction parameter for this blend is quite small, and it is apparently around $\chi_{PR} = -1.0 \times 10^{-3}$, though the exact value cannot be evaluated. Similar χ_{PR} with small absolute values were obtained for PP-1/D-EPR19a (80:20) and PP-1/D-EPR19b (60:40) as listed in Table 4.

The temperature dependence of χ_{PR} was also examined. SANS data for PP-1/D-EPR47b (60:40) and PP-1/D-EPR19b (60:40) at various temperatures are shown in Figures 5 and 8, respectively. Essentially no intensity change was observed within the temperature range 440 K $\le T \le$ 482 K. From these results it can be concluded that the temperature dependence of χ_{PR} in this temper-

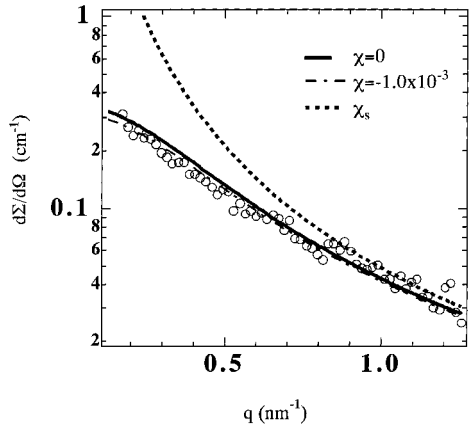

Figure 7. Background-corrected SANS intensities for PP-1/D-EPR19b (80:20) at 463 K. Solid and dotted lines have been calculated for $\chi = 0$ and for $\chi = \chi_s$. Dashed−dotted line corresponds to $\chi = -1.0 \times 10^{-3}$.

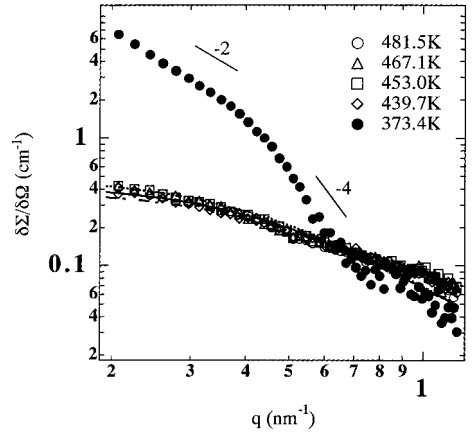

Figure 8. Background-corrected SANS intensities for PP-1/D-EPR19b (60:40) at different temperatures: 481.5 K (open circles), 467.1 K (open triangles), 453.4 K (open squares), 439.7 K (open diamonds), and 373.4 K (closed circles). Solid, dotted, and dashed−dotted lines have been calculated for $\chi = 0$, $\chi = 1.0 \times 10^{-3}$, and $\chi = -1.0 \times 10^{-3}$, respectively.

ature range is quite small for this blend system. In Figure 8 SANS data (closed circles) for PP-1/D-EPR19b at 373 K, to which the sample was gradually cooled after holding for 1 h at 439 K, are presented. The characteristic feature of phase separation can be observed. Two intensive scattering regions whose q dependences are $(d\Sigma/d\Omega \propto q^{-2} (q < 0.4\ nm^{-1})$ and $(d\Sigma/d\Omega) \propto q^{-4} (0.4 < q < 0.8\ nm^{-1})$ could be ascribed to domains and the interphase boundary, respectively. This fact is reasonably understood that the crystallization-induced phase separation occurred and that D-EPR19 was excluded from the crystalline phase of PP on crystallization because of the lack of crystallizability of EPR at that temperature.

Previous SANS results[13] indicate that the 50:50 blend of deuterated isotactic PP (M_w: 366 000) and EPR (M_w: 12 900, ethylene content: 12 wt %) was immiscible at 200 °C; however, it is difficult to compare the previous results with those of the present study because the samples used in the previous SANS experiments were the blend of deuterated isotactic PP and unlabeled EPRs.[40,41] Further, neither the microstructures nor the catalyst for polymerization of EPR was stated in ref 13.

Transmission electron micrographs for quenched samples from the melt are presented in Figure 9. The lamella structures are observed for PP-1 (Figure 9a),

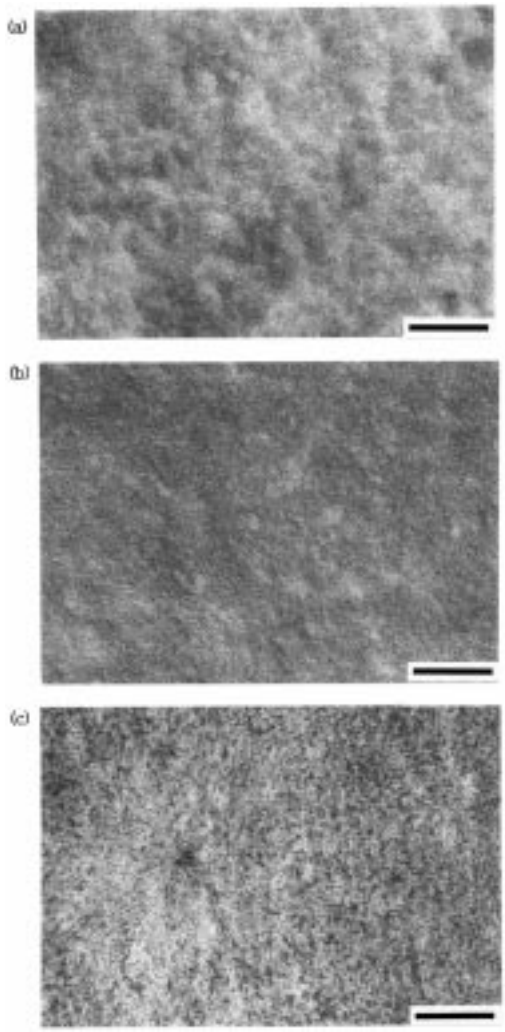

Figure 9. TEM images of the blends quenched from 493 K. Sample: (a) PP-1, (b) PP-1/D-EPR19b (80:20), and (c) PP-1/D-EPR47b (80:20). Scale bars are 0.2 μm.

PP-1/D-EPR19b (80:20) (Figure 9b), and PP-1/D-EPR47b (80:20) (Figure 9c), but no domain structure whose size is of the order of an optical microscope can be observed for these blends. TEM images for PP-1/D-EPR19b (60:40), which was crystallized isothermally at 373.4 K from the melt, are shown in Figure 10a,b. Apparently the two-phase structure can be observed in these figures. Ellipsoidal aggregates of PP crystallites are dispersed in the D-EPR19-rich matrix. These results support the SANS results qualitatively.

In Figure 11 background corrected SAXS data for PP-1, PP-1/D-EPR47b (80:20), and PP-1/D-EPR19b (80:20), which were crystallized isothermally at 373 K from the melt, are plotted against the scattering vector. The first peak position (q_m) of the SAXS data (marked by arrow) can be assigned to the average size of the interlamella distances (L), which is given by $2\pi/q_m$. L was 11.7, 13.1, and 12.7 nm for PP-1, PP-1/D-EPR19b (80:20), and PP-1/D-EPR47b (80:20), respectively. It was found that the blends have longer interlamella distance than PP-1. X_c determined by DSC was 55, 54, and 54% for PP-1, PP-1/D-EPR19b (80:20), and PP-1/D-EPR47b (80:20), respectively. The melting points of them were almost the same and were 418 K. These results from DSC indicate that the total amount of PP crystallite and mean lamellae thickness of PP-1 and the blends would not be affected by blending D-EPR. The increases of L for these

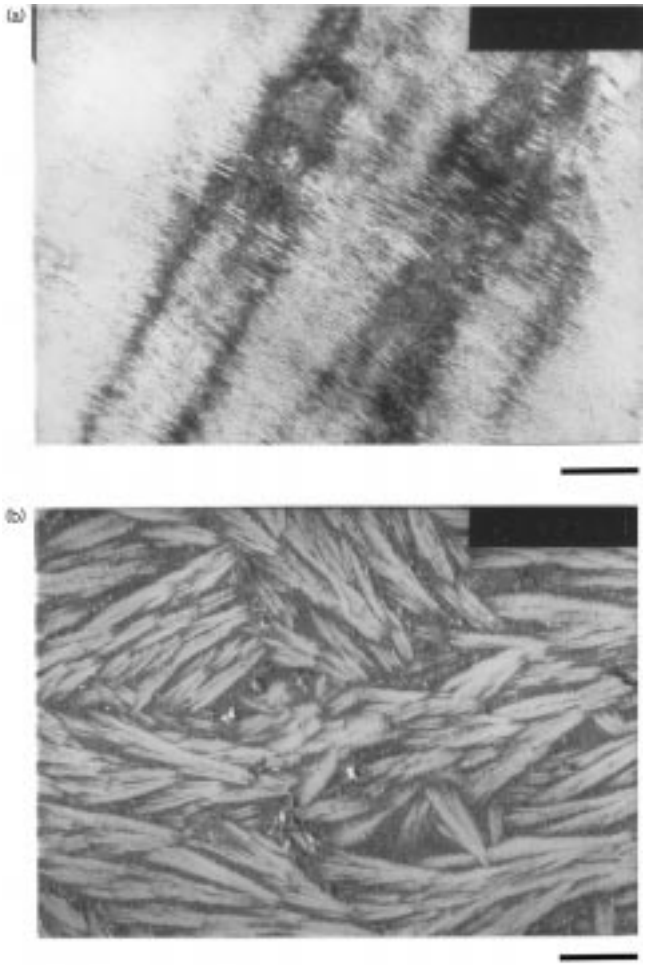

Figure 10. TEM images of PP-1/D-EPR19 (60:40) crystallized at 373.4 K for 1 h from the melt. Scale bars are (a) 0.2 μm and (b) 5.0 μm.

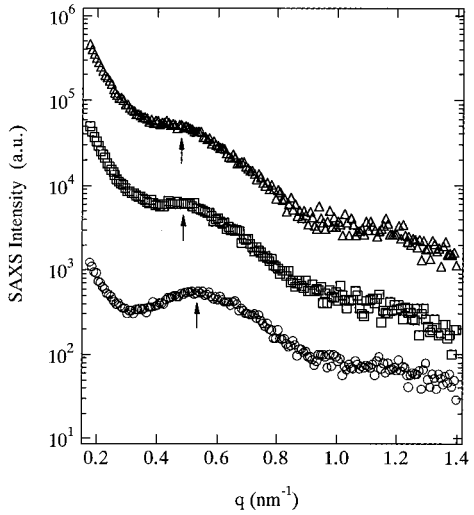

Figure 11. Background-corrected SAXS intensities from isothermally crystallized PP-1 (circles), PP-1/D-EPR19b (80:20) (squares), and PP-1/D-EPR47b(80:20) (triangles). Data sets have been shifted by a factor of 10 for clarity. The arrows indicate the peak position.

two blends would be due to the thickening of amorphous layers between the adjacent lamellae. This is probably caused by the results that D-EPR chains could not be excluded perfectly from the interlamella region on crystallization, and a certain amount of them was trapped in the amorphous layers between lamellae resulting in the increase of L.[42]

V. Conclusions and Summary

In this study we prepared the blends of isotactic PPs and D-EPRs, which were polymerized by metallocene catalyst and then fractionated. Both two blend series, i.e., PP/D-EPR47 and PP/D-EPR19, were confirmed to be homogeneous one-phase state in the melt by SANS, although we assumed the temperature dependence of R_g is negligible. χ_{PR} evaluated by SANS for PP/D-EPR47 blends is estimated to be approximately 5.0×10^{-3} while it is very small and within $-1.0 \times 10^{-3} \leq \chi_{PR} \leq 1.0 \times 10^{-3}$ for PP/D-EPR19. The temperature dependence of χ_{PR} within the temperature range $440 \leq T \leq 482$ K for these two systems was concluded to be very small since distinct difference in SANS intensities were not observed. No phase separation of the order of an optical microscope can be observed by TEM for the blends quenched from the melt. Coherent scattering intensities for the PP/D-EPR blend below the melting temperature of PP showed the characteristic feature of phase separation. The increases of interlamella distance determined by SAXS for the isothermally crystallized blends from the melt would be ascribed to the existence of D-EPR molecules in the amorphous layer between PP lamellae.

Acknowledgment. We thank Dr. T. Usami at MCC for helpful discussions on interpretation of the results of ^{13}C NMR and Mr. H. Uchida and Miss. Y. Hayashi for measurements of the molecular weight.

References and Notes

(1) Hill, M. J.; Barham, P. J.; Keller, A. *Polymer* **1992**, *33*, 2530.
(2) Alamo, R. G.; Londono, J. D.; Mandelkern, L.; Stehling, F. C.; Wignall, G. D. *Macromolecules* **1990**, *27*, 411.
(3) Krishnamoorti, R.; Graessley, W. W.; Balsara, N. P.; Lohse, D. J. *Macromolecules* **1994**, *27*, 3037.
(4) Graessley, W. W.; Krishnamoorti, R.; Balsara, N. P.; Butera, R. J.; Fetters, L. J.; Lohse, D. J.; Schulz, D. N.; Sissano, J. A. *Macromolecules* **1994**, *27*, 3896.
(5) Graessley, W. W.; Krishnamoorti, R.; Reichart, G. C.; Balsara, N. P.; Butera, R. J.; Fetters, L. J.; Lohse, D. J. *Macromolecules* **1995**, *28*, 1260.
(6) Krishnamoorti, R.; Graessley, W. W.; Dee, G. T.; Walsh, D. J.; Fetters, L. J.; Lohse, D. J. *Macromolecules* **1996**, *29*, 397.
(7) Reichart, G. C.; Graessley, W. W.; Register, R. A.; Krishnamoorti, R.; Lohse, D. J. *Macromolecules* **1997**, *30*, 3036.
(8) Weimann, P. A.; Johnes, T. D.; Hillmyer, M. A.; Bates, F. S.; Londono, J. D.; Melnichenko, Y.; Wignall, G. D.; Almdal, K. *Macromolecules* **1997**, *30*, 3560.
(9) Fredrickson, G. H.; Liu, A. J.; Bates, F. S. *Macromolecules* **1994**, *27*, 2503.
(10) Bates, F. S.; Scultz, F. F.; Roesdale, J. H. *Macromolecules* **1994**, *27*, 4263.
(11) Schweizer, K. S.; Singh, C. *Macromolecules* **1995**, *28*, 2063.
(12) Sheffold, F.; Budkowski, A.; Steiner, U.; Eiser, E.; Klein, J. *J. Chem. Phys.* **1996**, 104, 8795.
(13) Lohse, D. J. *Polym. Eng. Sci.* **1986**, *26*, 1500.
(14) Inaba, N.; Yamada, T.; Suzuki, S.; Hashimoto, T. *Macromolecules* **1988**, *21*, 407.
(15) Chen, C. Y.; Yunus, W. Md. Z. W.; Chiu, H. W.; Kyu, T. *Polymer* **1997**, *38*, 4433.
(16) Mirabella, F. M.; McFaddin, D. C. *Polymer* **1996**, *37*, 931.
(17) Sano, H.; Takao, U.; Nakagawa, H. *Polymer* **1986**, *27*, 1497.
(18) Cham, P. M.; Lee, T. H.; Marand, H. *Macromolecules* **1994**, *27*, 4263.
(19) D'Orazio, L.; Mancarella, C.; Martyscelli, E.; Sticotti, G.; Massari, P. *Polymer* **1993**, *34*, 3671.
(20) Yamaguchi, M.; Miyata, H.; Nitta, K. *J. Appl. Polym. Sci.* **1996**, *62*, 87.
(21) Thomann, R.; Kressler, J.; Rudolf, B.; Mülhaupt, R. *Polymer* **1996**, *37*, 2635.

(22) For recent reviews, see: Kaminsky, W.; Arndt, M. *Adv. Polym. Sci.* **1997**, *127*, 144. Bochmann, M. *J. Chem. Soc., Dalton Trans.* **1996**, 255. Grubbs, R. H.; Coataes, G. W. *Acc. Chem. Res.* **1996**, *29*, 85. Brintzinger, H. H.; Fisher, D.; Mülhaupt, R.; Rieger, B.; Waymouth, R. M. *Angew. Chem., Int. Ed. Engl.* **1995**, *34*, 1143. Marks, T. J. *Acc. Chem. Res.* **1992**, *25*, 57.
(23) Chen, H. N. *Macromolecules* **1984**, *17*, 1950.
(24) Kalinowski, H. O.; Berger, S.; Braun, S. *Carbon-13 NMR Spectroscopy*; John Wiley and Sons: New York, 1984.
(25) Brown, R. G. *J. Chem. Phys.* **1963**, *38*, 221.
(26) Ito, Y.; Imai, M.; Takahashi, S. *Physica B* **1995**, *213&214*, 889.
(27) Brandup, S.; Immergut, E. M. *Polymer Handbook*; Interscience: New York, 1975.
(28) Daoud, M.; Cotton, J. P.; Farnoux, B.; Jannink, G.; Jnnink, G.; Sarma, G.; Benoit, H.; Duplessix, R.; Picot, C.; de Gennes, P. G. *Macromolecules* **1975**, *8*, 804.
(29) Maconnachie, A.; Richards, R. W. *Polymer* **1978**, *19*, 739.
(30) Hayashi, H.; Flory, P. J.; Wignall, D. G. *Macromolecules* **1983**, *16*, 1328.
(31) Ulmann, R. *Annu. Rev. Mater. Sci.* **1980**, *10*, 261.
(32) de Gennes, P. G. *Scaling Concepts in Polymer Physics*; Conell University Press: New York, 1979.
(33) Debye, P. *J. Phys. Colloid Chem.* **1974**, *51*, 18.
(34) Guinier, A.; Fournet, G. *Small Angle Scattering of X-rays;* Wiley-Interscience: New York, 1955.
(35) Zirkel, A.; Urban, V.; Richter, D.; Fetters, L. J.; Huang, J. S.; Kampmann, R.; Hadjichristidis, N. *Macromolecules* **1992**, *25*, 6418.
(36) Zirkel, A.; Richter, D.; Pyckhout-Hittzen, W.; Fetters, L. J. *Macromolecules* **1992**, *25*, 954.
(37) Alamo, R. G.; Graessley, W. W.; Krishnamoorti, R.; Lohse, D. J.; Londono, J. D.; Manderkern, L.; Stehling, F. C.; Wignall, G. D. *Macromolecules* **1997**, *30*, 561.
(38) Ewen, J. *J. Am. Chem. Soc.* **1984**, *106*, 6355.
(39) Stehling, U.; Diebold, J.; Kirsten, R.; Röll, W.; Brintzinger, H. H.; Jüngeling, S.; Mülhaupt, R.; Langauser, F. *Organometallics* **1994**, *13*, 964.
(40) Rhee, J.; Crist, B. *J. Chem. Phys.* **1993**, *98*, 4174.
(41) Graessley, W. W.; Krishnamoorti, R.; Balsara, N. P.; Fetters, L. J.; Lohse, D. J.; Schulz, D. N.; Sissano, J. A. *Macromolecules* **1993**, *26*, 1137.
(42) Keith, H. D.; Padden, F. J. *J. Appl. Phys.* **1964**, *35*, 1270.

MA981254W